Soft Matter

The Polarizability Response of a Glass-Forming Liquid Reveals Intrabasin Motion and Interbasin Transitions on a Potential Energy Landscape

Journal:	*Soft Matter*
Manuscript ID	SM-ART-11-2019-002326.R1
Article Type:	Paper
Date Submitted by the Author:	30-Jan-2020
Complete List of Authors:	Bender, John; National Institute of Standards and Technology Zhi, Miaochan; NIST, Biosystems and Biomaterials Cicerone, Marcus; Georgia Institute of Technology, Chemistry; National Institute of Standards and Technology, Biosystems and Biomaterials

Soft Matter

FULL PAPER

Cite this: DOI: 00.0000/xxxxxxxxxx

The Polarizability Response of a Glass-Forming Liquid Reveals Intrabasin Motion and Interbasin Transitions on a Potential Energy Landscape†

John S. Bender,[a] Miaochan Zhi,[a] and Marcus T. Cicerone[a,b‡]

Received Date
Accepted Date

DOI: 00.0000/xxxxxxxxxx

Potential energy landscape (PEL) concepts have been useful in conceptualizing the effects of intermolecular interactions on dynamic and thermodynamic properties of liquids and glasses. Primary features of the PEL are "basins", regions of reduced free energy associated with locally-preferred molecular packing. The molecular configurations at the bottom of these basins are referred to as inherent structures (ISs). Experimental methods for directly characterizing PEL features such as these are rare, largely relegating PEL concepts to theory and simulation studies, and impeding their exploration in real systems. Recently, we showed that quasielastic neutron scattering (QENS) data from propylene carbonate (PC) exhibits signatures of picosecond timescale motion that are consistent with intrabasin motion and interbasin transitions [Cicerone, *et al., J. Chem. Phys.* 2017, 146, 054502]. Here we present optically-heterodyne-detected optical Kerr effect (OHD-OKE) spectroscopy studies on PC. The data exhibit signatures of motion within and transitions between basins that agree quantitatively with and extend the QENS results. We show that the librational component of the OKE response corresponds to intrabasin dynamics, and the enigmatic intermediate OKE response corresponds to interbasin transition events. The OKE data extend the measurement range of these parameters and reveals their utility in characterizing PEL features of real systems.

1 Introduction

Amorphous condensed matter, including liquids and glassy solids, exhibits a range of dynamic processes occurring on time scales spanning many orders of magnitude. At THz frequencies, these systems feature a nearly temperature-independent "β_{fast}" process associated with quasi-ballistic rattling of molecules or atoms against one another. On the other end of the dynamic scale is the highly temperature-dependent α relaxation. This process is associated with viscous flow and is Arrhenius at sufficiently high temperatures but becomes subtly super-Arrhenius below some temperature, T_A, well above the melting point.[1] At a lower temperature, typically denoted T_c, the α relaxation begins to become noticeably super-Arrhenius and appears to bifurcate into two relaxation processes. The faster of these is referred to as the Johari-Goldstein β relaxation,[2] or β_{JG}, and is thought to be a precursor to the α process.

The underlying cause of super-Arrhenius slowing of the α process near the glass transition temperature has for decades been an active area of experimental and theoretical exploration. A number of theoretical approaches[3–9] seek to account for the α behavior based on the properties of fast, localized dynamic processes. While timescales for the proposed localized relaxations are not always specified, they seem to be broadly compatible with β_{fast} processes observed experimentally. Taking a slightly different approach, Goldstein proposed that the increase in apparent activation energy for α relaxation results from a crossover to activated dynamics, where flow-related dynamic processes begin to significantly sample an underlying potential energy landscape (PEL) at reduced temperatures.[10] This idea has since been developed extensively for supercooled liquids and glass.[11–14]

For a liquid or glass of N atoms or molecules at constant pressure, a PEL is a $3N$ dimensional hypersurface that encodes the system's thermodynamic and dynamic information. Figure 1 shows a cartoon representation of a one-dimensional cut through a PEL. Although the overall surface is highly dimensional, many of the important features (including basins and metabasins) involve just a few, spatially localized particles,[15] so the abscissa in Figure 1 can be thought of as rearrangement among a small number of

[a] *Address, National Institute of Standards and Technology, Gaithersburg, MD 20899, U.S.A.*
[b] *Address, Department of Chemistry and Biochemistry, Georgia Institute of Technology, Atlanta, GA 30332, U.S.A. Tel: 01 404 894 2761; E-mail: cicerone@gatech.edu*
‡ To whom correspondence should be sent.
† Electronic Supplementary Information (ESI) available: [Contains extended experimental and data fitting detail, along with tables of all parameter fits and uncertainties]. See DOI: 10.1039/cXsm00000x/

particles. "Inherent structures" (ISs), are locally stable configurations. Elastic deformations of these stable structures raise the potential energy, giving rise to basins. Molecular motions responsible for basin exploration are small-scale collective vibration or rattling of molecules in a cage of its neighbors. These intrabasin (NB) motions at the bottom of the basins compose the vibrational component of the β_{fast} process.[16] Their timescale and lengthscale (σ_{IS} in Fig. 1) are encoded by the PEL curvature at the basin minima. Likewise, transits across interbasin (IB) barriers occur on a timescale and lengthscale (σ_{IB} in Fig. 1) determined by the local curvature at the top of these barriers, and related to the distance between basins.[17] This barrier transit motion is slightly slower than the "cage rattling" and comprises the relaxation component of the β_{fast} process.[16]

Transitions between basins (basin barrier transits followed by reorganization into a new IS) involve potentially non-reversing collective rearrangements of a small number of particles[18,19] and give rise to the β_{JG} relaxation.[16,20] These IB transitions constitute the most fundamental relaxation process in an amorphous system.

Basins are thought to be organized into groups, or "metabasins" (MBs), that must be transitioned between for complete rearrangement of local structure (i.e., α relaxation). At high temperatures, IB transitions and α relaxation (putative transitions between metabasins) occur on nearly the same timescales[16]. However, at temperatures below T_c, the aggregated basin structure is thought to become important,[21] and systems may become temporarily localized in a particular MB, leading to a bifurcation between α and β_{JG} relaxation times. IB transitions may occur as string-like events in this temperature regime, and this behavior may be fundamental to spatially heterogeneous dynamics.[18,22]

The PEL and its features connect to dynamic and thermodynamic properties of liquids and glasses. For example, the curvature at the bottom of the basins determines the vibrational density of states, the number of ISs as a function of energy determines the configurational heat capacity, and the barriers between basins determine structural relaxation rates.[14] The PEL concept is equally valid for simple liquids and more complex systems such as biomolecules,[23] and amorphous, glassy materials.[24–28] However, there are few instances of experimental measurements being explicitly connected to the topographical features of the PEL. As with any theoretical construct, verification (through measurement) of key concepts is necessary to guide its development. The PEL formalism has found wide use and has been verified in many aspects through simulation, but has minimal direct experimental constraint.

We recently used quasielastic neutron scattering (QENS) to show that β_{fast} relaxation dynamics in several glass-forming liquids is composed of two separate processes occurring on distinct timescales and lengthscales,[16,29,30] corresponding to basin exploration and basin barrier crossing events. Additionally, we showed that β_{JG} relaxation is equivalent to transitions between basins.[16] Consistent with our conclusions, Bin *et al.*[20] subsequently found that β_{JG} events occur spatially in string-like fashion, as is expected for basin transition events.

Here we investigate how these distinct processes manifest in optical Kerr effect (OKE) spectroscopy, which is a time-domain implementation of depolarized light scattering. OKE spectroscopy is complimentary to QENS in several ways. OKE has a slightly better time resolution (10s of fs) compared to QENS (typically 500 fs), and also has higher dynamic range in that it can detect motion of a smaller fraction of molecules. This allows us to carry meaningful measurements out at lower temperature (as demonstrated in Fig. 6 B). Being an optical technique, it is somewhat more accessible than neutron scattering. This is especially true since OKE is the time-domain equivalent of depolarized light scattering, so studies related to the present one could be carried out even with commercially available apparatus. Further, we hereby make a connection between PEL features and previously performed depolarized light scattering experiments in liquids.

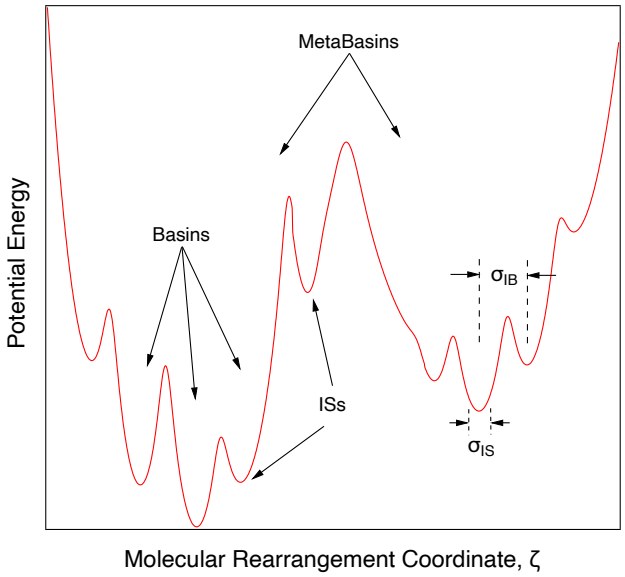

Fig. 1 Cartoon representation of a one-dimensional slice taken through a 3N dimensional potential energy landscape (PEL), along some coordinate representing rearrangement of a small group of spatially adjacent molecules in some nano-volume of a liquid. σ_{IB} and σ_{IS} respectively represent the distance between basins and the typical excursions within a basin that give rise to time-dependent blurring of the inherent states.

OKE and light scattering techniques have been used extensively to characterize dynamics in liquids.[31–39] Data from such experiments have typically been analyzed in terms of mode-coupling models,[36,40–44] and to our knowledge, have not previously been considered in terms of PEL-related dynamics. Mode-coupling does predict a β_{fast} process, but does not anticipate the two distinct relaxation processes observed on this timescale in QENS studies.[16,29]

The OKE response of liquids generally contains a fast component associated with molecular libration, and a slightly slower "intermediate" component, followed by α relaxation. While an intermediate response is generally found, its origin remains unclear, and reports of its behavior vary considerably. For example, Fourkas *et al.*[45] and Ricci *et al.*[46] found relaxation times that scaled with viscosity for several symmetric top liquids. On the other hand, Kakinuma and Shirota[47] studied several six-

membered-ring liquids and found that the intermediate responses occurred on a $\approx$ 1 ps timescale, apparently independent of viscosity. Additionally, Fayer *et al.*[33,48] found a temperature-independent, picosecond timescale intermediate relaxation process for 2-ethylnaphthalene. Despite the conflicting results concerning connection to the bulk response, that it is thought to be related to the local structure of the liquid seems to be a consistent theme. We emphasize that the "intermediate relaxation" process we refer to here is a picosecond timescale process, and not the >100 ps timescale intermediate process shown to be related to β_{JG} relaxation.[34,35]

In this work, we measure the collective polarizability dynamics of propylene carbonate (PC) using optically-heterodyne-detected OKE (OHD-OKE) spectroscopy. We present compelling evidence that the picosecond timescale dynamic phenomena observed, molecular libration and intermediate relaxation, correspond to basin exploration and IB barrier crossing events respectively. The OKE results agree quantitatively with previous QENS characterization of these motions.[16] This work extends these measurements to lower temperatures revealing key PEL characteristics, and demonstrates how these parameters may be obtained with optical methods such as OKE and, by extension, depolarized light scattering.[34,35]

1.1 Model of OHD-OKE Response

The OHD-OKE signal, $S(t')$, is encoded with the Raman-active intermolecular and intramolecular modes of the interrogated system. $S(t')$ is proportional to the convolution of an instrument response function, $G(t)$, and the third-order nonlinear optical response, $R^{(3)}(t)$, of the interrogated system:

$$S(t') \propto \int_{-\infty}^{\infty} \mathrm{d}t G(t) R^{(3)}(t-t'), \tag{1}$$

where t' is the delay between the probe and pump pulses. Well-known deconvolution techniques allow the extraction of $R^{(3)}(t)$ from $S(t')$ so long as $G(t)$ is measured accurately.[41,49,50] $R^{(3)}(t)$ is the sum of the instantaneous electronic response and the non-instantaneous nuclear response, $R_{nuc}(t)$, which is the negative time derivative of the collective polarizability time correlation function (TCF). We model $R_{nuc}(t)$, excluding dynamic coupling, as the sum of component responses:

$$R_{nuc}(t) = \sum_i A_i R_i(t), \tag{2}$$

where A_i is the amplitude of the response, R_i is the response, and the index includes librational (l), "intermediate" (c), intramolecular (v), and diffusive (d) components.

At the longest timescales, the diffusive component of the polarizability TCF is often modeled by the Kohlrausch-Williams-Watts (KWW) function in glass-forming liquids. Assuming this is an appropriate representation, we model $R_d(t)$ as

$$R_d(t) = \frac{\beta_{KWW}}{t}\left(\frac{t}{\tau_d}\right)^{\beta_{KWW}} e^{-\left(\frac{t}{\tau_d}\right)^{\beta_{KWW}}} \times \left[1 - e^{-\left(\frac{t}{\tau_{rise}}\right)}\right]\theta(t), \tag{3}$$

where τ_d is the relaxation time constant, β_{KWW} is the stretching exponent, τ_{rise} is the rise time of the dynamics, and $\theta(t)$ is the Heavyside step function, which preserves causality. $R_d(t)$ dominates $R_{nuc}(t)$ at times greater than several picoseconds and can persist to times more than 10 orders of magnitude later for glassy materials.

The intermediate response decays on a significantly shorter time scale, lasting up to several picoseconds. This response is typically exponential in character,[33,45,47] and we model it according to

$$R_c(t) = e^{-\left(\frac{t}{\tau_c}\right)}\left[1 - e^{-\left(\frac{t}{\tau_{rise}}\right)}\right]\theta(t), \tag{4}$$

where τ_c is the relaxation time constant. Simulations show that collision-induced dynamics decay on a timescale similar to that of the intermediate response, typically up to a few picoseconds for van der Waals liquids.[51–53] It is worth noting, then, that the intermediate response may be a result of these dynamics and would therefore be expected to be collective in nature.

The librational component of $R_{nuc}(t)$ dominates the response at times up to about a picosecond and is the result of hindered molecular rotations as molecules explore their cage composed of neighboring molecules. Due to inhomogeneous broadening, this response may be modeled as a distribution of coherently driven quantum harmonic oscillators:[54–56]

$$R_l(t) = e^{-\left(\frac{t}{\tau_l}\right)} \int_0^{\infty} \frac{\sin(\omega t)}{\omega} g(\omega)\mathrm{d}\omega\theta(t), \tag{5}$$

where τ_l is the pure dephasing time, and $g(\omega)$ is the distribution of oscillators. We have chosen the usual antisymmetrized Gaussian (AG) distribution,[54,55,57] which is given as

$$g(\omega) = e^{-\frac{(\omega-\omega_l)^2}{2\sigma^2}} - e^{-\frac{(\omega+\omega_l)^2}{2\sigma^2}}, \tag{6}$$

where ω_l is the central frequency and σ is the spectral width of the constituent Gaussian functions.

In addition to these responses, any intramolecular mode with a vibrational frequency within the bandwidth of the excitation pulse will contribute to $R_{nuc}(t)$. This oscillatory response can be approximated as a classical underdamped harmonic oscillator:

$$R_v(t) = e^{-\frac{gt}{2}}\cos(\omega_v t - \phi)\theta(t), \tag{7}$$

where g is the damping coefficient, ω_v is the vibrational frequency, and ϕ is the induced phase change relative to the driving force.

In our analysis, we normalize each response, $R_i(t)$, according to

$$\int_{-\infty}^{\infty} R_i(t)\mathrm{d}t = 1. \tag{8}$$

Amplitude values, A_i reported herein reflect this normalization.

2 Experimental

2.1 OHD-OKE Setup

A schematic representation of the OHD-OKE setup is shown in Figure 2. A 4.5 W portion of a 532 nm continuous wave laser (Coherent, Verdi V-5) pumps a Kerr-lens-locked Ti:Sapphire oscillator (KMLabs, Griffin). The oscillator produces ∼480 mW average power with a ∼5.5 nJ pulse, and a nearly Gaussian spectrum centered at ∼800 nm. The oscillator pulse train seeds a regenerative amplifier (KMLabs, Wyvern-500), which produces ∼ 5.6 W of average power and pulse energies of ∼56 μJ.

A 1.0 W portion of the output beam is filtered spatially and delivered to a pulse shaping module (Biophotonics, MIIPS-HD) for dispersion compensation. After precompensation, the pulse width measured at the sample position was ∼35 fs. The shaped beam is then split with a 3 mm wedge, where the probe beam is reflected and the pump beam is transmitted.

The pump beam is transmitted through a half-wave plate and a Glan-Laser polarizer, where it is polarized vertically. It is then amplitude modulated at 1 kHz with an optical chopper (Thorlabs MC2000) and focused through the sample with a 50 cm lens, after which it is terminated with a beam block.

The probe beam is reflected down a 250 mm delay stage (Newport, ILS250HA) equipped with a linear encoder and motion controller (Newport, ESP 301), where a piezo-adjusted mirror retro reflects the beam back through the 3 mm wedge. A continuous wave laser (OEM Laser Systems) is propagated along the same path as the probe on the delay, and its position is monitored by terminating it onto a quadrant detector (Thorlabs, PDQ80A), which is interfaced with an auto-positioning software suite and piezo-controllers (Thorlabs, APT, KPZ101). Each axis of the piezo-adjusted mirror is controlled to maintain the alignment of the probe beam throughout the range of the delay stage. After the delay stage, the probe beam is transmitted through a half-wave plate and a Glan-Laser polarizer, where it is polarized 45° relative to the pump polarization. The probe is focused through the sample with a 30 cm lens at the same point as the pump beam, recollimated, and circularly polarized with a quarter-wave plate. A Wollaston prism then separates the horizontal and vertical components of the probe beam. These components are fiber coupled to a balanced detector (New Focus, Nirvana 2007), where the horizontal component is subtracted from the vertical. This detection scheme, developed by Giraud *et al.*, produces an automatically heterodyned signal, where the homodyne and local oscillator contributions are removed on a per pulse basis.[58] The resultant signal is recovered with a lock-in amplifier (Stanford Research Systems, SR830), referenced to the frequency of a beam chopper.

The sample is mounted onto the cold finger of a research cryostat (Janis, CCS450). The temperature of the cryostat is controlled to within 1 K by a cryogenic temperature controller (Lake Shore, Model 335). The cryostat is positioned such that the sample contains the entire interaction volume of the crossed pump and probe beams.

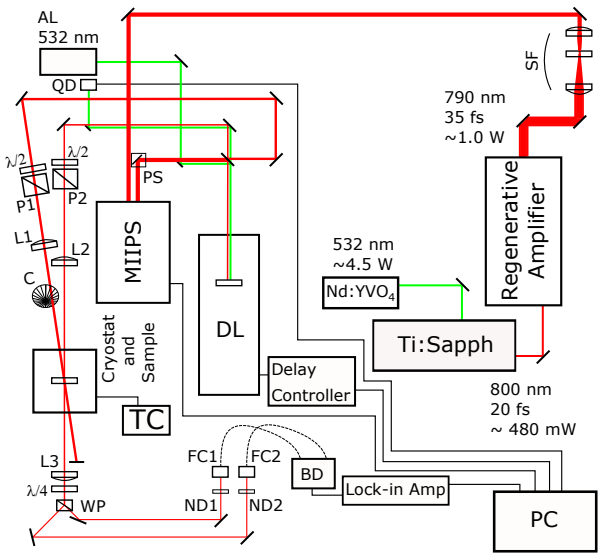

Fig. 2 Schematic layout of the ultrafast OHD-OKE spectrometer. SF = spatial filter, PS = periscope, AL = alignment laser, QD = quad detector, DL = delay line, P = polarizer, C = chopper, L= lens, TC = temperature controller, WP = Wollaston prism, ND = neutral density filter, FC = fiber coupler, BD = balanced detector, PC = personal computer

2.2 Sample Preparation

Anhydrous propylene carbonate (Sigma-Aldrich) was passed through a 0.22 μm filter into a cylindrical, 2 mm pathlength cuvette (Starna Cells, 37-Q-2). The liquid was degassed with several freeze-pump-thaw cycles, and the cuvette was flame sealed under vacuum upon the final freeze. The sealed cuvette was secured to a custom fabricated brass mount, which was attached to the cold finger of the cryostat.

2.3 Data Collection

Two types of data scans were performed at each temperature investigated: one for the short-time dynamics and one for the long-time. For all scans, the average probe power at the sample position was set to ∼ 1.5 mW and the pump power was set to ∼ 23.5 mW. Ten short-time scans were performed up to 10 ps by scanning the delay line continuously at 0.01 mm/s. The position of the delay was polled every 70 ms, corresponding to a 0.7 μm step. At least 30 long-time scans were performed at 10× the speed of the short-time scans at each temperature. The collected long-time response was allowed to decay to the baseline. The collected data, which had small deviations in delay step size, were then interpolated linearly to have constant spacing at 5 fs intervals before they were averaged. The long-time data were then scaled and spliced to the short-time data to produce a full decay at each temperature.

2.4 Instrumental Response Function Measurement

The accurate measurement of the instrument response function is crucial to the subsequent analysis of short-time, fast dynamics. We used the methodology developed by Taschin *et al.* to measure the instrument response function.[41,59] We made the reference sample by inserting a 2.0 mm thick CaF_2 window into an

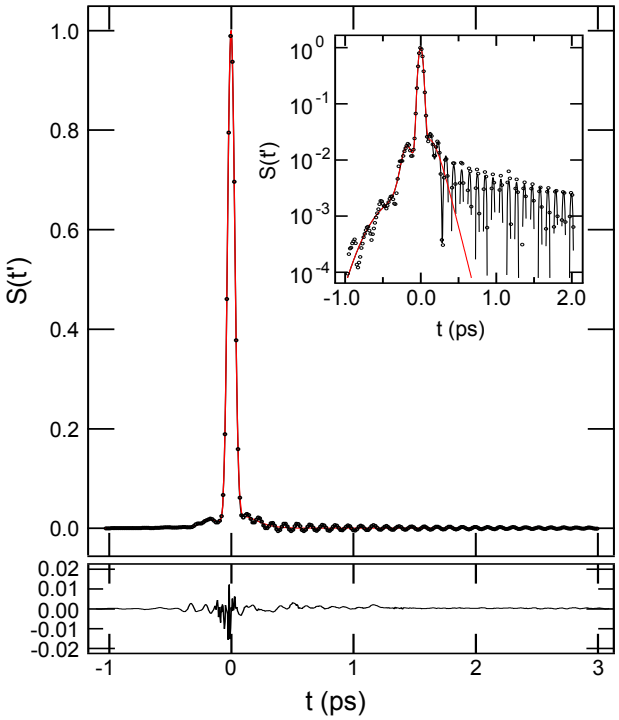

Fig. 3 Normalized OHD-OKE decay for CaF_2. The experimental data (open circles), fit (black line), and extracted instrument response, $G(t)$, (red line) are shown in the top panel. The inset is the same plot on a semi-logarithmic scale. The residuals of the fit are shown in the bottom panel.

identical cuvette as that used in the experiment. To eliminate etalon effects between the surfaces of the window and the cuvette, an index matching glue (Norland Products, NOA144) was used to eliminate the interfaces. The refractive index of the glue (1.44) was chosen to fall between that of quartz (1.46) and CaF_2 (1.43).

The reference sample was mounted with the experimental sample on the same brass holder in the cryostat. Before and after each experimental scan, the OHD-OKE response of the CaF_2 reference was measured under identical geometric and thermal conditions by taking ten short-time scans. The CaF_2 responses were interpolated and averaged in the same manner as the experimental responses, to produce a CaF_2 response with identical time step spacing.

To extract the instrument response function, the CaF_2 response was fit to Eq 1, where $R_{nuc}(t)$ was modeled as an underdamped harmonic oscillator corresponding to an intramolecular mode at $322\,cm^{-1}$, and $G(t)$ was modeled as the sum of several Gaussian and $sech^2$ functions. A nonlinear least squares regression using the Levenberg-Marquardt algorithm was used to fit the response. This process was particularly import for these experiments as the instrument response function had significant structure. Figure 3 shows the measured CaF_2 response (open circles) and the fit to Eq 1 (black line). The extracted $G(t)$ (red line) captures any asymmetry and structure in the low intensity wings of the pulse.

2.5 Determination of Fit Parameters

The raw, long-time tails (10 ps and longer) of the responses for PC were fit to Eq 3 and its associated amplitude to arrive at the diffusive relaxation time constant and stretching parameters. The total decays were then deconvoluted according to the procedure outlined in the Supplementary Material to arrive at the nuclear responses. The initial peak of $R_{nuc}(t)$, which is dominated by librational dynamics, was normalized to unity and then fit to the model described in the text using the Levenberg-Marquardt nonlinear least squares fitting procedure.

All parameters were adjusted freely except τ_d and β_{KWW}, which were extracted from the initial fits to the long-time tail. The diffusive component was below the noise floor for the responses at 130K and 150 K. The fitted $R_{nuc}(t)$ functions were then convoluted with $G(t)$ extracted from the CaF_2 response (see Section 2.4 above). In accordance with Eq 1, the summation of these functions was added to $G(t)$, and the total function was scaled to produce the fit to the OHD-OKE signals. An example of the total fit for PC at 310 K is shown in Figure S2. This fitting procedure was performed for the entire set of data, moving sequentially from low temperature to high temperature, using the previous set of fitted parameters as the initial guess for the next. The procedure was repeated going from high temperature to low temperature, and the fitted parameters were found to be consistent. The initial guess for the first response analyzed was constructed graphically.

3 Results and Discussion

Figure 4A shows a log-log plot of the normalized OHD-OKE responses for PC at several temperatures as solid black lines. The fits to these data using Eq. 1 are shown as solid colored lines (violet to red as temperature increases). Once the nuclear and instrument responses are deconvolved and $R_d(t)$ (the α relaxation) is removed, a response function remains that subtly but systematically varies with temperature. In Fig. 4B, deconvolved responses are amplitude scaled two 1.0, and $R_d(t)$ is subsequently removed. As demonstrated clearly in Fig. 5A, these response functions are comprised of three components. A large amplitude librational component dominates the early time response and is followed by a weaker, exponentially rising and falling intermediate response. At longer times an intramolecular vibrational mode becomes the dominant feature and appears as an underdamped oscillation.

Figure 5A shows an example of the dynamic model fit to the $R_{nuc}(t)$ of PC at 295 K with $R_d(t)$ removed. The model provides for an accurate description of the data as is seen by inspection of the residuals in the lower inset. As discussed above, $R_l(t)$ dominates the short time response, whereas $R_c(t)$ is the dominant contributor at longer times. The oscillatory response, $R_v(t)$, is due to the intramolecular mode (out-of-plane ring deformation) centered at $\approx 190\,cm^{-1}$. We recovered no temperature dependent behavior for $R_v(t)$ other than the expected linear blue shift of its center frequency with decreasing temperature.

The diffusive and vibrational dynamics are easily separated from $R_{nuc}(t)$ as their functional forms and timescales are quite distinct from $R_l(t)$ and $R_c(t)$. Separating the librational and intermediate dynamics is more challenging as their response functions are somewhat similar, and their timescales overlap. In spite of

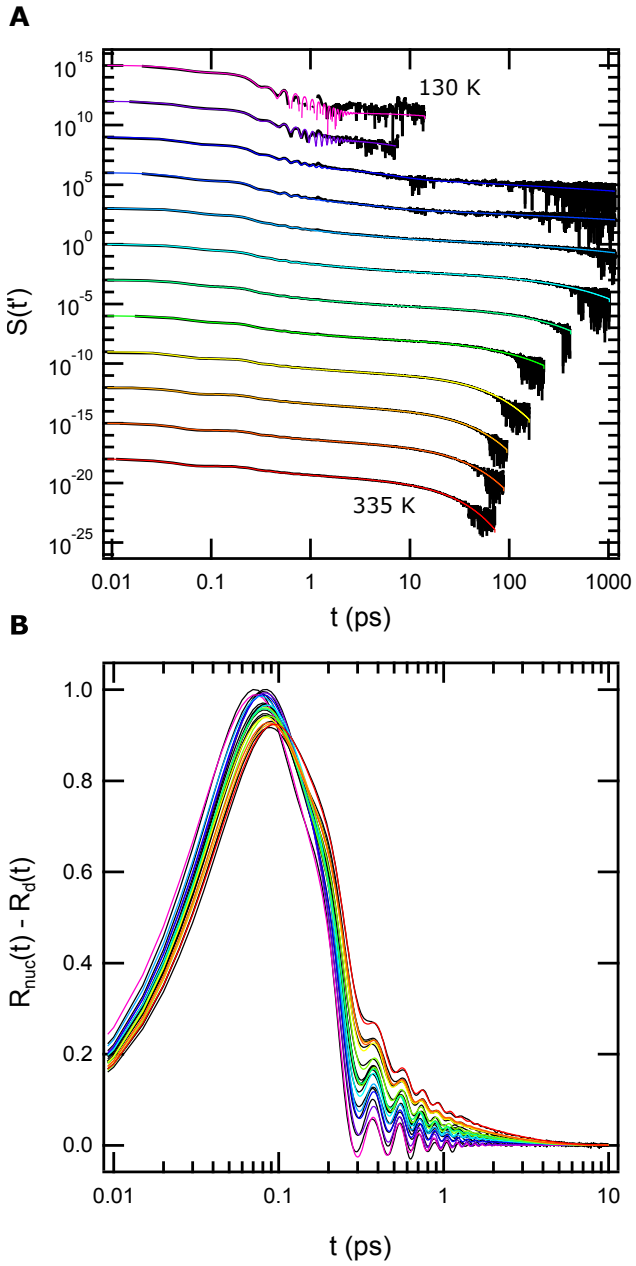

Fig. 4 (A) Normalized OHD-OKE decays for PC at 130 K, 150 K, 170 K, 185 K, 210 K, 240 K, 265 K, 295 K, 310 K, 320 K, and 335 K. The black lines are experimental data, and the colored lines are fits to the model described in the text (Eq 1). Temperature is increasing from violet to red. Decays are offset for clarity. (B) Reduced nuclear responses. Black lines are experimental data and colored lines are fits. Colors are the same as in (A).

this difficulty, two distinct responses within the 10ps range are ubiquitously found in the OKE response of liquids.[33,47,48,60,61]

3.1 Equivalence of $\{\langle\tau_l\rangle, \tau_c\}$ and $\{\tau_{NB}, \tau_{IB}\}$

Figure 5B shows $R_{nuc}(t)$ with $R_d(t)$ and $R_v(t)$ removed. At short times we obtain a strong, nearly temperature-independent response that gives way at longer times to a smaller amplitude, but strongly temperature dependent response. Evidence for two separate response functions at t <10 ps is seen ubiquitously in OKE studies.[33,47,48,51–53,60–62] We associate the slower response with collective motion, $R_c(t)$, and, as usual, associate the faster response with molecular libration, $R_l(t)$. For clarity in Fig. 5B we normalize $R_l(t)$ amplitudes to 1, and scale the corresponding $R_c(t)$ fits by the same $R_l(t)$ normalizing factors (this temperature-dependent scaling is not used in Fig. 6A). This minor scaling helps to clarify that, consistent with previous reports, we observe narrowing and a shift to longer time in the librational response (i.e. broadening and a shift to lower frequency in the librational susceptibility, see Fig. 7.) with increasing temperature. Although slowing-down in the dynamics with higher temperature may seem counter-intuitive, it is simply a result of slightly lower packing density and the system sampling greater anharmonicity in the inter-molecular potentials. Additionally, the amplitude of the intermediate response increases with increasing temperature.

Separation of the response function at <10 ps into two distinct processes is commonly done for OKE data. It is also supported by results of recent QENS studies on PC,[16] where we found two distinct responses in the β_{fast} process. We identified the faster process with molecular "rattling" within a cage of its neighbors - exploration within basins on a PEL and the slower process as barrier crossing events between two contiguous PEL basins. Below we show that the temperature dependence in timescale and amplitude of the PEL dynamics derived from QENS correspond to those obtained from the present OKE study.

Figure 6A compares temperature-dependent amplitudes of the intermediate relaxation from OKE with the instantaneous number of IB barrier crossing events from QENS. Specifically, the QENS results report on the number fraction of PC molecules involved in an IB transition in any 1 ps time window (Φ_0).[29] In Fig 6A we have multiplied the amplitudes of A_c by a constant factor so that they overlap Φ_0 values on this graph. The temperature dependence of the two parameters are identical to within experimental uncertainty, suggesting that the intermediate relaxation seen in OKE arises from barrier crossing events in IB transitions. The timescales of the measured responses also supports this conclusion.

Figure 6B shows temperature dependence of characteristic timescales for both of the fast relaxation components measured by OKE and by QENS. From the OKE data we plot the first moment of the librational response $R_l(t)$, $\langle\tau_l\rangle$, along with τ_c from the intermediate response in filled and hollow red circles. Here we see that the OKE-derived $\langle\tau_l\rangle$ and τ_c values are indistinguishable from QENS-derived[16] τ_{NB} and τ_{IB} respectively, suggesting that the two approaches provide metrics of similar motions.

In addition to identical timescales and amplitude trends, we

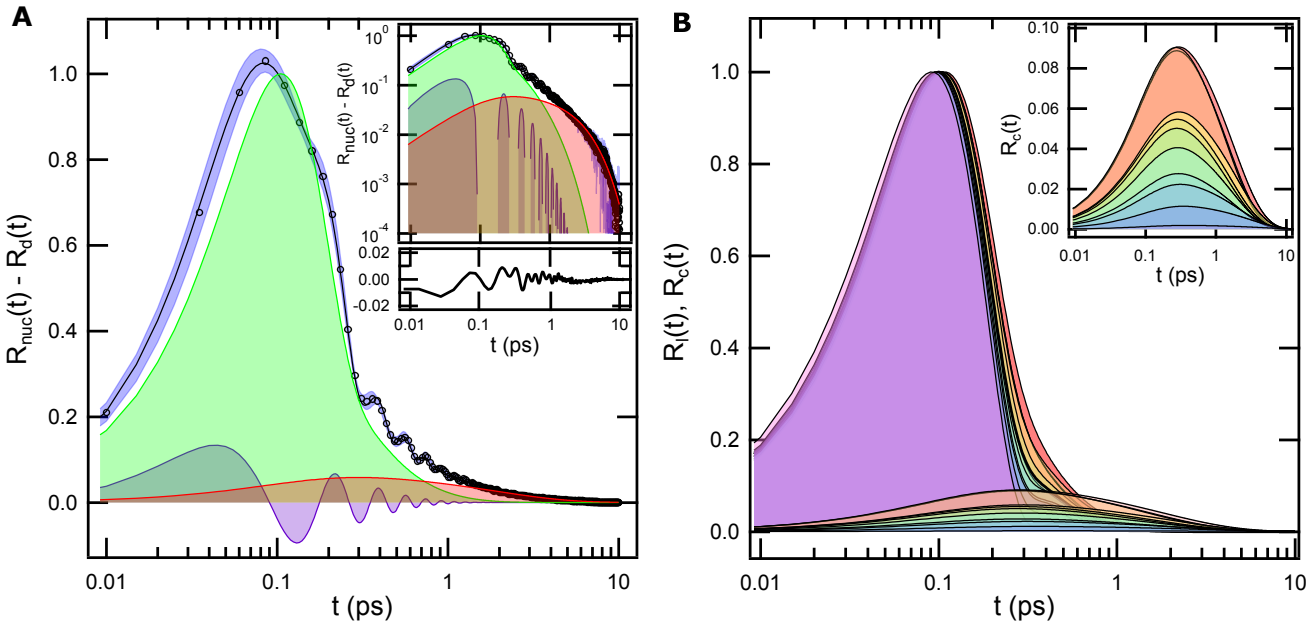

Fig. 5 (A) Example of modeled data for PC at 295 K. (Top) Experimental (open circles), $R_{nuc}(t)$ (black line), $R_l(t)$ (green area), $R_c(t)$ (red area), and $R_v(t)$ (violet area) responses. The blue area represents error in the measurement at one standard deviation taken from multiple single decay measurements. (Inset) Semi-logarithmic plot (top) of responses and residuals to the fit (bottom). (B) Librational (peaked at $\approx 100\,\mathrm{fs}$) and intermediate (peaked at $\approx 350\,\mathrm{fs}$) responses underlying fits to experimental data at temperatures ranging from 130 K to 335 K (colors correspond to those of Figure 4). (Inset) Expanded view of the temperature-dependent $R_c(t)$.

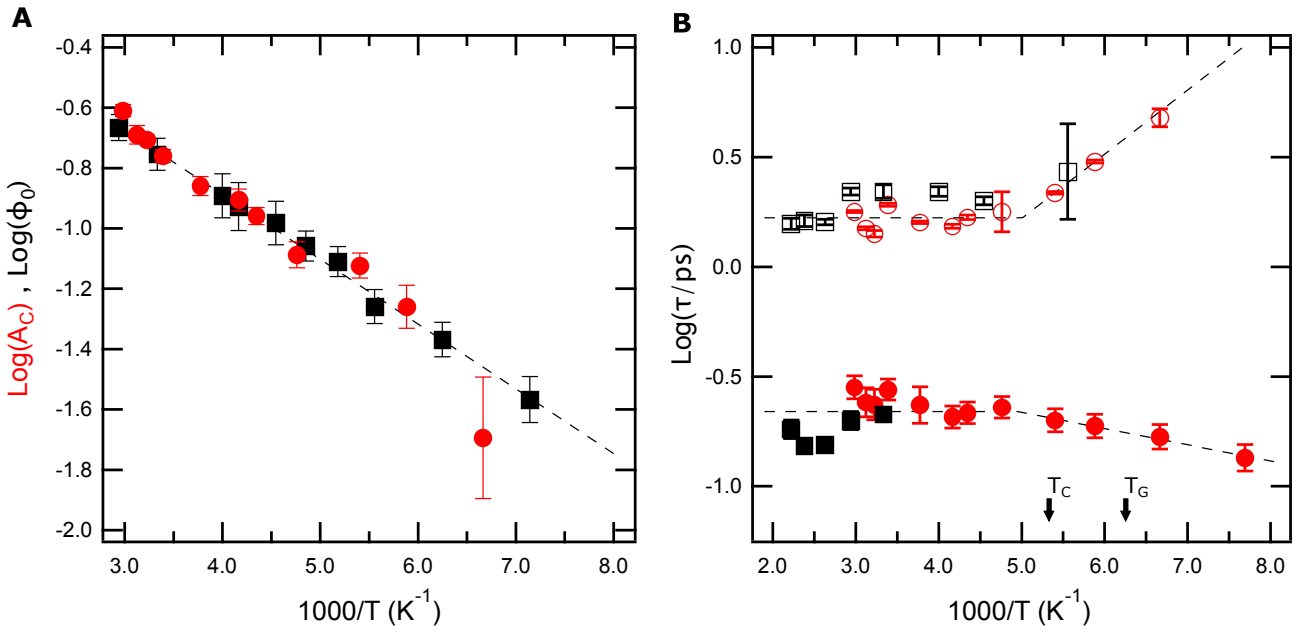

Fig. 6 Timescales and amplitudes extracted from fits of the nuclear responses to Eq 4 and Eq 5. (A) $Log[A_c]$ (red circles) and $Log[\Phi_0]$ (black squares, taken from ref. 29) as a function of $1000/T$. (B) τ_c (open red circles), τ_{IB} (open black squares, taken from ref. 29), $\langle\tau_l\rangle$ (filled red circles), and τ_{NB} (filled black squares taken from ref. 29) as a function of $1000/T$.

find support for the idea that OKE and QENS responses report on the same dynamic processes from the similarity in the detailed nature of responses of these processes. It is well known that librational and NB motion arise from elastic deformations of local structure.[46,63] NB motion, colloquially referred to as "rattling in a cage", has an essentially temperature-independent amplitude, and it is the primary contributor to the β_{fast} response. The "rattling" leads to fluctuations in the local environment, but neither it nor any faster processes lead to irreversible relaxation. Correspondingly, from OKE response literature, Kubo analysis suggests that librational dynamics are not motionally narrowed,[46] so there are no faster processes that lead to significant environmental fluctuations, and librational motion itself does not directly lead to relaxation (i.e., environmental modifications).

Likewise, the OKE "intermediate relaxation" and IB barrier crossings have similar properties. IB barrier crossing involves collective translational motion on a characteristic lengthscale of approximately 20% of the molecule's hydrodynamic radius.[16,18] These motions will necessarily be encoded on the collision-induced component of the OHD-OKE response which exhibits an exponential decay with $\tau_c \approx 1$ ps[33,47,48,51–53,60–62] as observed here, and as observed for τ_{IB} from QENS. Further, the intermediate response is known to arise from motionally narrowed intermolecular modes.[45,46] Correspondingly, hopping between basins is essentially the movement of molecules from one local (inherent) structure to the next as a cage is broken and subsequently reformed after a relatively large excursion occurs. This sampling of local structures would lead to motional narrowing as the rearranged particles sample the heterogeneous landscape. In addition to these points of evidence, the temperature dependence of $\langle\tau_l\rangle$ and τ_c are consistent with expectations for NB motion and IB transitions.

The fact that $\langle\tau_l\rangle$ and τ_c do not arise from motion associated with hydrodynamic modes is clear since the characteristic timescales plotted in Fig. 6B are essentially independent of temperature in the range between 450 K and 200 K, where viscosity changes by three orders of magnitude. By contrast, values for these parameters begin to change at temperatures below 200 $\pm$3 K, just where the direct influence of the PEL is expected to emerge. We have previously argued that τ_{IB} from QENS is the timescale for barrier crossing between PEL basins.[16] Here we extend that association to τ_c, implying that it reports on curvature at the top of IB barriers. If we couple this implication with the assumption that barrier curvature and well depth are positively correlated,[17] the data suggest that dynamics are increasingly dominated by transitions between enthalpically shallower wells at T < 200 K. This suggestion can only mean that the system is less frequently transitioning between deeper wells, but rather becoming trapped within them, as is expected in the PEL framework.[21] We suspect that the change in temperature dependence of $\langle\tau_l\rangle$ may have a related origin, which we explore below in context of other libration-related parameters.

Figure 7 shows ω_l and σ for $R_l(t)$, plotted with respect to temperature. Their temperature dependencies can be largely understood by indications from simulation that ω_l is related to density and σ is postitively correlated with thermal energy content

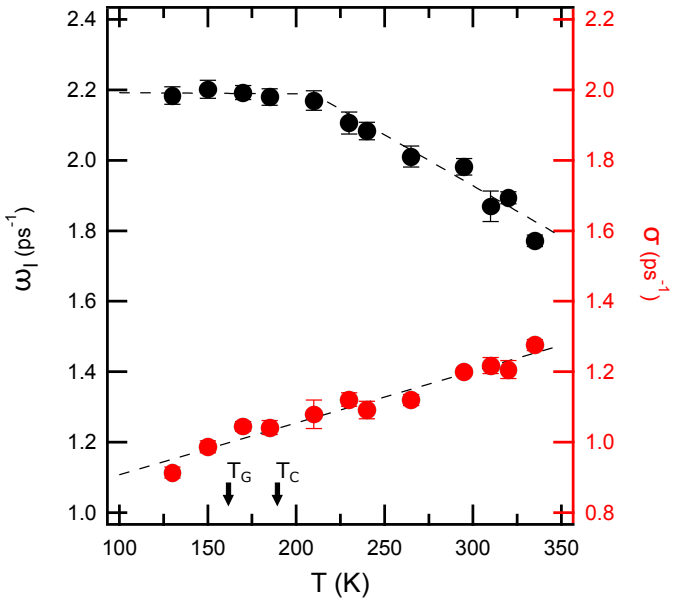

Fig. 7 Spectral components extracted from fits of the nuclear responses to Eq 5. ω_l (black circles) and σ (red circles) plotted as a function of T. The dashed lines are linear regressions to the data, and the error bars represent one standard deviation taken from the fit to Eq (5).

of the liquid.[64] An increase in density corresponds to a stiffer intermolecular potential, causing a blue shift in the librational frequency, whereas a decrease in temperature narrows the librational spectrum as a result of a decrease in population of high energy states. This simple reasoning leads one to anticipate a reduction in the temperature dependence of ω_l near T_g = 157 K where the liquid drops out of structural equilibrium and cannot fully densify with further temperature reduction. Interestingly, we observe such a change at a much higher temperature, 205$\pm$10 K. While a change in temperature dependence near T_c is hard to understand from an overall average density perspective, it is consistent with observed IS behavior.

Sastry *et al.*[65] found that below T_c liquids sample a low-energy, narrow, and temperature-independent distribution of inherent structures. Near T_c they found this distribution began to increase in breadth and average energy with increasing temperature. The observed behavior of ω_l is consistent with this behavior since it is temperature independent below T_c, but decreases at higher temperature where increased IS energy implies lower density packing and thus lower expected vibrational frequency,[11] as well as greater anharmonicity.

We can now connect the behavior of $\langle\tau_l\rangle$ values plotted in Fig. 6B to the PEL. $\langle\tau_l\rangle$ is the first moment average of $R_l(t)$, which is in turn a function of ω_l and σ. At T < 200 K ω_l is roughly temperature independent while σ increases with temperature. This leads to a positive correlation in changes of T and $\langle\tau_l\rangle$ in this range because increases in σ are due primarily to increased spectral amplitude on the low frequency side of the distribution. Physically, this suggests that softer modes begin to be sampled more frequently at higher temperatures. At temperatures above 200 K, opposing changes in ω_l and σ appear to have a mutually offsetting effect

on $\langle\tau_l\rangle$, as it is essentially temperature independent in this range.

As the temperature is increased above T_c, higher energy IS configurations become accessible, but this trend terminates at a higher temperature, just above T_A, and the distribution of available states again becomes nearly independent of temperature.[11,66] We see from Fig. 5B that the modes newly accessible with increasing temperature are preferentially soft, and will thus be associated with increased anharmonicity. Accordingly, one expects an enhanced temperature dependence in the characteristic lengthscale of NB motions between T_c and T_A. We observed this behavior previously in QENS experiments for PC and several other liquids,[16,29] and it has also been observed in simulation of model systems.[67] From our previous work,[29] we expect this high-temperature turnover to evolve over the range (400 to 450) K. Experimental data reported here cover a range approaching but not quite overlapping this anticipated transition. However, an impending high-temperature transition is consistent with implications of β_{KWW} fit parameters discussed below.

3.2 β_{KWW} Stretching Exponent

It is widely accepted that spatially and temporally heterogeneous dynamics underlie stretched relaxation behavior in liquids and glasses, leading to $\beta_{KWW} < 1$ in Eq. (3). In principle then, onset of $\beta_{KWW} < 1$ should signal the temperature at which the PEL barriers leading to heterogeneous dynamics become important[65] and the temperature dependence of β_{KWW} should give us clues to the nature of those relaxation barriers.[9,21,68,69]

While β_{KWW} parameters are potentially very informative, they are notoriously difficult to measure with high precision. A stretched exponential relaxation function with the modest value of β_{KWW}=0.5 has significant spectral amplitude over roughly 4 orders of magnitude in frequency.[70] Additionally, at high temperatures the high-frequency tail of this distribution can approach the THz range and nearly merge with β_{fast} processes. High-fidelity fits in the time or frequency domain depend on properly capturing even the full relaxation spectrum and properly rejecting the fast β relaxation. Insufficient measurement bandwidth will lead to β_{KWW} values that are artificially large with potentially weak temperature dependence, and incompletely rejecting β_{fast} motion will lead to artificially small values.

The OKE instrument used here is well-suited for correctly extracting $\beta_{KWW} \geq 0.5$ since it provides roughly 4 orders of magnitude dynamic range in sensitivity over 4.5 orders of magnitude in frequency (here, 30 to .001 THz). Furthermore, OKE allows fitting in the time domain, making it quite straightforward to reject β_{fast} effects by simply starting α relaxation fits at 10 ps, when β_{fast} motion is completely relaxed. Reports of β_{KWW} parameters from experiments on PC range widely from a temperature-independent value extracted from light scattering,[40,71] to more-or-less monotonically decreasing values with reduced temperature in light scattering and dielectric spectroscopy.[72–74] Supplemental Fig. S3, shows that β_{KWW} values reported here have a similar temperature dependence to, but are are generally smaller than β_{KWW} values reported elsewhere for PC, suggesting that the present measurements more faithfully capture the full α relaxation spectrum.

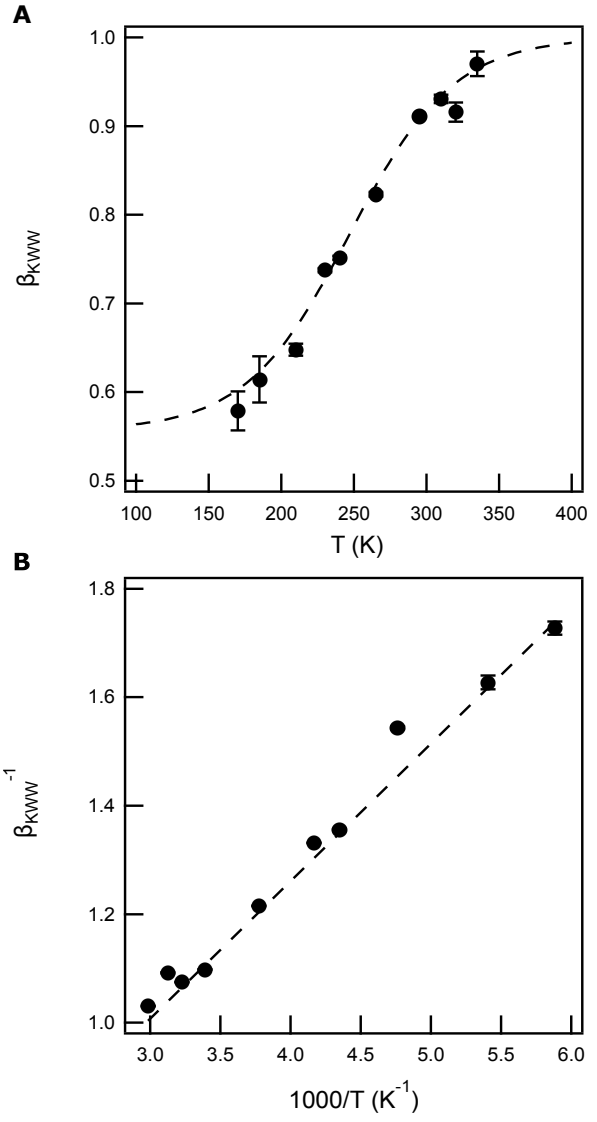

Fig. 8 (A) β_{KWW} vs T. The dashed line is a sigmoidal fit to the data. (B) $1/\beta_{KWW}$ vs 1000/T. The dashed lines are linear regressions to the data. Error bars represent one standard deviation taken from the fit to Eq. (3).

Figure 8 shows β_{KWW} plotted against temperature in two formats, suggested by different theoretical constructs.[9,21] Douglas et al.[9] envision dynamic heterogeneity through transient intermolecular associations that persist on the timescale of measurement. Under a simple ansatz accounting for entropic and enthalpic effects, they anticipate a sigmoidal increase in β_{KWW} with temperature, as shown in panel A. Stillinger,[21] on the other hand proposed a scenario in which $\beta_{KWW}^{-1} \propto T^{-1}$ as shown in panel B, and in which emergence of collective motion is described through the concept of basin collections. These basin collections, or metabasins (MBs) are separated by free energy barriers (η). By construction, transitions between the MBs lead to α relaxation, and the super-Arrhenius temperature dependence of τ_α is accounted for with η values that increase as temperature is low-

ered. Increases in η naturally leads to a larger number of basins aggregated in a single MB. In his treatment, Stillinger proposed that

$$\beta_{KWW}^{-1} = 1 + \gamma q^{-1} + (q k_B T)^{-1} \quad (9)$$

where γ and q are material-specific parameters that dictate the temperature dependence of metabasin size and transition rates between metabasins.

It seems we cannot discriminate between these two models based only on quality of fit to the data. However, the fit parameters do provide some useful information. The inflection point in the sigmoidal fit is 244±6 K, just a few degrees above where we observe the break in temperature dependence of ω_l. This is not in any sense in direct support of the Douglas model, but it does suggest potential constraints on how the model can be interpreted. Likewise, while the fits to the Stillinger model are qualitatively reasonable, parameter fit values, $\gamma = -(1.58 kJ/mol)^{-1}$ and $q = (2.10 kJ/mol)^{-1}$ lead to problems for the theoretical framework. Several expressions in the model, such as for the temperature dependence of η, have exponents containing $[(\gamma + (k_B T)^{-1}]$. Since γ is negative, and roughly equal to $(k_B T)^{-1}$, this leads to singularities in key expressions. In fact, the only way to avoid this is for β_{KWW}^{-1} to approach 1 only as T approaches ∞.

In spite of the relatively high precision with which β_{KWW} parameters can be extracted from OKE data, it is important to remember that the OKE relaxation function records the polarizability response of the liquid, which will reflect the asymmetry of the molecule. Given that the polarizability and rotational diffusion tensors of PC are anisotropic due to multiple inertial axes of the molecule, the diffusive component of the OKE response could be composed of up to five exponential functions[75] so that β_{KWW} values could be <1 even when the liquid dynamics are homogeneous. As a case in point, one might expect $\beta_{KWW} = 1$ at $T > T_A$, $\approx 280K$ for PC.[1] From our experimental data for PC, it is impossible to say whether the deviations of β_{KWW} from 1 at $T > T_A$ are due to persistent heterogeneous dynamics of the liquid, or whether they are due to molecular anisotropy. Accounting for the anisotropy of the polarizability tensor in the diffusive component of the OKE response data will require significant effort, including comparison to simulation, but will be worthwhile as it will provide improved accuracy in the extracted information about the statistical properties of the PEL.[21,68,69]

Along these lines, since the OKE librational spectrum corresponds to NB dynamics, it gives access to the vibrational density of states (VDOS) and in principle allows one to directly obtain the vibrational entropy of the liquid. However, the Raman spectrum is a weighted representation of the VDOS, and one needs a knowledge of the temperature dependence of the spectral weighting factors. As with the β_{KWW} parameters, supplementary data (here, QENS) would allow these weighting factors to be determined. Although this idea is outside the scope of this work, being able to calculate the vibrational entropy from OHD-OKE experiments could prove useful in determining the contribution of the intermolecular vibrational entropy to the total excess entropy of a supercooled liquid or glass.

4 Conclusions

By performing OHD-OKE experiments on PC over a wide range of temperatures and comparing results to previously reported QENS data, we show that the librational and intermediate OKE responses correspond respectively and quantitatively to intrabasin motion and interbasin barrier crossings on a PEL.

In the 5 decades or so since PEL ideas were first introduced by Goldstein,[10] many experimental papers have invoked PEL ideas, but we are aware of only two other experimental measurements in liquids that specifically identify landscape characteristics. In one, Stillinger[76] enumerated ISs from heat capacity data for o-terphenyl. The other is our previous QENS work.[16]

To our knowledge, this is the first time OKE data have been described in terms of the PEL formalism, connecting simple dynamic models to the potential energy topography of the liquid. The OKE fit parameters provide information over a wide temperature range related to specific aspects of the PEL for actual materials. The PEL characteristics probed include curvature at the top of potential barriers between basins and the subset of these barriers that are sampled at a given temperature. The fit parameters also provide information about potential energy depth and anharmonicity of the populated ISs. Through these OKE measurements, we have characterized important aspects of the local PEL topography for PC. We expect that additional aspects of the PEL, such as MB features, will also be accessible through OKE and similar approaches through carefully characterizing the long-time α relaxation behavior.

We believe the demonstration of an accessible experimental method for acquiring PEL parameters in real systems will open a new window on refining PEL ideas and facilitate a more solid connection between them and macroscopic material characteristics.

Conflicts of interest

There are no conflicts to declare.

Acknowledgements

J.S.B. thanks the National Research Council for a Postdoctoral Research Fellowship through the Research Associate Program.

Official contributions of the National Institute of Standards and Technology. Not subject to copyright in the United States.

References

1 F. Stickel, E. W. Fischer and R. Richert, *J. Chem. Phys.*, 1996, **104**, 2043–2055.
2 G. P. Johari and M. Goldstein, *J. Chem. Phys.*, 1970, **53**, 2372–2388.
3 J. P. Garrahan and D. Chandler, *Phys. Rev. Lett.*, 2002, **89**, 035704.
4 A. S. Keys, J. P. Garrahan and D. Chandler, *PNAS*, 2013, **110**, 4482–4487.
5 T. R. Kirkpatrick, D. Thirumalai and P. G. Wolynes, *Phys. Rev. A*, 1989, **40**, 1045–1054.
6 X. Xia and P. G. Wolynes, *PNAS*, 2000, **97**, 2990.

7 X. Xia and P. G. Wolynes, *Phys. Rev. Lett.*, 2001, **86**, 5526–5529.

8 K. L. Ngai, *J. Phys. Chem. B*, 1999, **103**, 5895–5902.

9 E. B. Stukalin, J. F. Douglas and K. F. Freed, *J. Chem. Phys.*, 2008, **129**, 094901.

10 M. Goldstein, *J. Chem. Phys.*, 1969, **51**, 3728–3739.

11 S. Sastry, *Nature*, 2001, **409**, 164.

12 P. G. Debenedetti and F. H. Stillinger, *Nature*, 2001, **410**, 259.

13 M. D. Ediger and P. Harrowell, *J. Chem. Phys.*, 2012, **137**, 080901.

14 P. K. Gupta and W. Kob, *J. Non-Cryst. Solids: X*, 2019, **3**, 100031.

15 T. F. Middleton and D. J. Wales, *Phys. Rev. B*, 2001, **64**, 024205 EP –.

16 M. T. Cicerone and M. Tyagi, *J. Chem. Phys.*, 2017, **146**, 054502.

17 R. W. Hall and P. G. Wolynes, *J. Chem. Phys.*, 1987, **86**, 2943–2948.

18 M. Vogel, B. Doliwa, A. Heuer and S. C. Glotzer, *J. Chem. Phys.*, 2004, **120**, 4404–4414.

19 G. A. Appignanesi, J. A. Rodríguez Fris, R. A. Montani and W. Kob, *Phys. Rev. Lett.*, 2006, **96**, 057801.

20 H.-B. Yu, R. Richert and K. Samwer, *Sci. Adv.*, 2017, **3**, e1701577.

21 F. H. Stillinger, *Phys. Rev. B*, 1990, **41**, 2409–2416.

22 B. A. Pazmiño Betancourt, F. W. Starr and J. F. Douglas, *J. Chem. Phys.*, 2018, **148**, 104508.

23 D. Wales, *Energy Landscapes: Applications to Clusters, Biomolecules and Glasses*, Cambridge University Press, 2003.

24 A. Saksaengwijit, J. Reinisch and A. Heuer, *Phys. Rev. Lett.*, 2004, **93**, 235701.

25 B. Doliwa and A. Heuer, *Phys. Rev. Lett.*, 2003, **91**, 235501.

26 E. La Nave, H. E. Stanley and F. Sciortino, *Phys. Rev. Lett.*, 2002, **88**, 035501.

27 I. Saika-Voivod, F. Sciortino and P. H. Poole, *Phys. Rev. E*, 2004, **69**, 041503.

28 T. B. Schrøder, S. Sastry, J. C. Dyre and S. C. Glotzer, *J. Chem. Phys.*, 2000, **112**, 9834–9840.

29 M. T. Cicerone, Q. Zhong and M. Tyagi, *Phys. Rev. Lett.*, 2014, **113**, 117801.

30 M. T. Cicerone, D. Averett and J. J. de Pablo, *J. Non-Cryst. Solids*, 2015, **407**, 118–125.

31 H. Cang, V. N. Novikov and M. D. Fayer, *Phys. Rev. Lett.*, 2003, **90**, 197401.

32 G. Li, M. Fuchs, W. M. Du, A. Latz, N. J. Tao, J. Hernandez, W. Götze and H. Z. Cummins, *J. Non-Cryst. Solids*, 1994, **172-174**, 43–51.

33 S. Greenfield, A. Sengupta, J. J. Stankus and M. Fayer, *Chem. Phys. Lett.*, 1992, **193**, 49–54.

34 A. Brodin and E. A. Rössler, *J. Chem. Phys.*, 2006, **125**, 114502.

35 A. Brodin and E. A. Rössler, *J. Chem. Phys.*, 2007, **126**, 244508.

36 J. Wuttke, M. Ohl, M. Goldammer, S. Roth, U. Schneider, P. Lunkenheimer, R. Kahn, B. Rufflé, R. Lechner and M. A. Berg, *Phys. Rev. E*, 2000, **61**, 2730–2740.

37 S. Kinoshita, Y. Kai, M. Yamaguchi and T. Yagi, *Phys. Rev. Lett.*, 1995, **75**, 148–151.

38 Q. Zhong and J. T. Fourkas, *J. Phys. Chem. B*, 2008, **112**, 15529–15539.

39 N. T. Hunt, A. A. Jaye and S. R. Meech, *Phys. Chem. Chem. Phys.*, 2007, **9**, 2167–2180.

40 W. M. Du, G. Li, H. Z. Cummins, M. Fuchs, J. Toulouse and L. A. Knauss, *Phys. Rev. E*, 1994, **49**, 2192–2205.

41 A. Taschin, P. Bartolini, R. Eramo, R. Righini and R. Torre, *Nat. Commun.*, 2013, **4**, 2401.

42 G. Hinze, D. D. Brace, S. D. Gottke and M. D. Fayer, *J. Chem. Phys.*, 2000, **113**, 3723–3733.

43 G. Hinze, D. D. Brace, S. D. Gottke and M. D. Fayer, *Phys. Rev. Lett.*, 2000, **84**, 2437–2440.

44 R. Torre, P. Bartolini and R. M. Pick, *Phys. Rev. E*, 1998, **57**, 1912–1920.

45 B. J. Loughnane, A. Scodinu, R. A. Farrer, J. T. Fourkas and U. Mohanty, *J. Chem. Phys.*, 1999, **111**, 2686–2694.

46 M. Ricci, P. Bartolini, R. Chelli, G. Cardini, S. Califano and R. Righini, *Phys. Chem. Chem. Phys.*, 2001, **3**, 2795–2802.

47 S. Kakinuma and H. Shirota, *J. Phys. Chem. B*, 2015, **119**, 4713–4724.

48 S. Greenfield, A. Sengupta, J. J. Stankus, M. Terazima and M. Fayer, *J. Phys. Chem.*, 1994, **98**, 313–320.

49 D. McMorrow, *Opt. Commun.*, 1991, **86**, 236–244.

50 D. McMorrow and W. T. Lotshaw, *J. Phys. Chem.*, 1991, **95**, 10395–10406.

51 J. S. Bender, B. Coasne and J. T. Fourkas, *J. Phys. Chem. B*, 2015, **119**, 9345–9358.

52 M. D. Elola and B. M. Ladanyi, *J. Chem. Phys.*, 2005, **122**, 224506.

53 M. D. Elola and B. M. Ladanyi, *J. Phys. Chem. B*, 2006, **110**, 15525–15541.

54 D. McMorrow, N. Thantu, V. Kleiman, J. S. Melinger and W. T. Lotshaw, *J. Phys. Chem. A*, 2001, **105**, 7960–7972.

55 M. Reichert, H. Hu, M. R. Ferdinandus, M. Seidel, P. Zhao, T. R. Ensley, D. Peceli, J. M. Reed, D. A. Fishman, S. Webster, D. J. Hagan and E. W. V. Stryland, *Optica*, 2014, **1**, 436–445.

56 P. Zhao, M. Reichert, S. Benis, D. J. Hagan and E. W. V. Stryland, *Optica*, 2018, **5**, 583–594.

57 Y. J. Chang and E. W. Castner, *J. Phys. Chem.*, 1996, **100**, 3330–3343.

58 G. Giraud, C. M. Gordon, I. R. Dunkin and K. Wynne, *J. Chem. Phys.*, 2003, **119**, 464–477.

59 A. Taschin, P. Bartolini, R. Eramo, R. Righini and R. Torre, *J. Chem. Phys.*, 2014, **141**, 084507.

60 D. McMorrow and W. T. Lotshaw, *Chem. Phys. Lett.*, 1990, **174**, 85–94.

61 D. McMorrow, W. T. Lotshaw and G. A. Kenney-Wallace, *IEEE J. Quantum Electron.*, 1988, **24**, 443–454.

62 B. M. Ladanyi and Y. Q. Liang, *J. Chem. Phys.*, 1995, **103**,

6325–6332.
63 D. J. Wales and J. P. K. Doye, *Phys. Rev. B*, 2001, **63**, 214204.
64 J. S. Bender, S. R. Cohen, X. He, J. T. Fourkas and B. Coasne, *J. Phys. Chem. B*, 2016, **120**, 9103–9114.
65 S. Sastry, P. G. Debenedetti and F. H. Stillinger, *Nature*, 1998, **393**, 554.
66 Y. Brumer and D. R. Reichman, *Phys. Rev. E*, 2004, **69**, 041202.
67 J. Hernández-Rojas and D. J. Wales, *J. Non-Cryst. Solids*, 2004, **336**, 218–222.
68 M. F. Shlesinger and E. W. Montroll, *PNAS*, 1984, **81**, 1280–1283.
69 J. L. Skinner, *J.Chem. Phys.*, 1983, **79**, 1955–1964.
70 C. P. Lindsey and G. D. Patterson, *J. Chem. Phys.*, 1980, **73**, 3348–3357.
71 M. Elmroth, L. Börjesson and L. M. Torell, *Phys. Rev. Lett.*, 1992, **68**, 79–82.
72 A. Schönhals, F. Kremer, A. Hofmann, E. W. Fischer and E. Schlosser, *Phys. Rev. Lett.*, 1993, **70**, 3459–3462.
73 U. Schneider, P. Lunkenheimer, R. Brand and A. Loidl, *Phys. Rev. E*, 1999, **59**, 6924–6936.
74 A. Brodin and E. A. Rössler, *J. Phys.: Condens. Matter*, 2006, **18**, 8481–8492.
75 B. J. Berne and R. Pecora, *Dynamic Light Scattering: with Applications to Chemistry, Biology, and Physics*, Courier Corporation, 2000.
76 F. H. Stillinger, *J. Phys. Chem. B*, 1998, **102**, 2807–2810.